CHEMISTRY OF MATERIALS | 25th Anniversary

Communication

Solution-Phase Synthesis of Highly Conductive Tungsten Diselenide Nanosheets

Priscilla D. Antunez, David H. Webber, and Richard L. Brutchey

Chem. Mater., **Just Accepted Manuscript** • DOI: 10.1021/cm400790z • Publication Date (Web): 30 May 2013

Solution-Phase Synthesis of Highly Conductive Tungsten Diselenide Nanosheets

Priscilla D. Antunez, David H. Webber, and Richard L. Brutchey*

Department of Chemistry and the Center for Energy Nanoscience and Technology, University of Southern California, Los Angeles, California 90089-0744, United States

KEYWORDS tungsten diselenide, WSe_2, nanosheet, transition metal dichalcogenide, layered material, conductivity

Early transition metal dichalcogenides are an important class of layered materials that have been used for hydrogen storage, transistors, lubricants, catalysis, capacitors, batteries, and photovoltaic devices.[1] The structure of transition metal dichalcogenides consists of repeating crystalline layers, which are responsible for their 2D anisotropic physical properties. Notable properties of transition metal dichalcogenides include superconducting behavior in $NbSe_2$ and TaS_2,[2] and the observation of ultralow thermal conductivities (0.05 W m^{-1} K^{-1}) in disordered WSe_2 crystals.[3] In the nanoscale regime, transition metal dichalcogenides have recently been shown to exhibit properties that make them particularly interesting when compared to bulk material. For example, MoS_2 nanotubes are more air stable and exhibit greater loading capacities of Li than in the bulk.[4] Moreover, certain transition metal dichalcogenides have been shown to change from indirect to direct band gap semiconductors when isolated as single layers.[5]

Bulk tungsten diselenide (WSe_2) is an indirect semiconductor that can be doped to generate a *p*- or *n*-type type material.[6] Bulk WSe_2 possesses a band gap of $E_{g\ \mathrm{indir}}$ = 1.2 eV,[7] a high absorption coefficient, and high photostability.[6a] In addition, its incorporation into photoelectrochemical devices has resulted in conversion efficiencies up to 17% (J_{SC} = 38 mA cm^{-2}).[8] Bulk WSe_2 exhibits hole carrier concentrations of 3.88×10^{17} cm^{-3} and highly anisotropic conductivities that range between 0.7 and 6.0 S cm^{-1} for in-plane measurements.[9] Tungsten diselenide crystallizes in Se-W-Se layers where tungsten coordinates through strong covalent-ionic (*ca.* 13% fractional ionic character) bonds to six selenium atoms in a trigonal prismatic geometry.[10] Variations in layer stacking results in different polytypes; the 2H-WSe_2 polytype refers to the two layers and the hexagonal structure represented in one unit cell, corresponding to the hexagonal molybdenite structure ($P6_3/mmc$).[11]

Traditional methods to prepare WSe_2 include sputtering, chemical vapor transport, solid-state reactions, and electrodeposition;[12] however, there have been very few reports of solution-phase syntheses of colloidal WSe_2 nanostructures. In 2000, Huang *et al.* synthesized 4-7 nm WSe_2 nanoparticles by the reaction of H_2Se with WCl_4 dissolved in a ternary tridodecylmethylammonium iodide/hexane/octane inverse micelle solution.[13] In 2004, Duphil *et al.* synthesized WSe_2 nanoparticles by the reaction of elemental Se with $W(CO)_6$ dissolved in *p*-xylene at 140 °C for several hours.[14] The resulting 10-30 nm nanoparticles were then annealed at 550 °C, with XRD patterns revealing crystalline tungsten oxide impurities. Herein, we present the first report of a facile solution-phase synthesis of colloidal WSe_2 nanosheets.

Diorganodichalcogenides have proven to be useful chalcogen sources for the facile solution-phase synthesis of colloidal semiconductor nanocrystals.[15] The synthesis of WSe_2 nanosheets was achieved by the injection of 185 µL (0.92 mmol) di-*tert*-butyl diselenide ($^tBu_2Se_2$) into a solution of 150 mg (0.46 mmol) WCl_4 in 25 mL dodecylamine at 150 °C under nitrogen. The solution was then heated to 225 °C and held at this temperature for 6 h prior to quenching. Tetra-*n*-octylammonium bromide (TOAB) was added during the work-up to prevent agglomeration of the nanosheets, following an adapted version of a previously published method.[16] The final washed product was highly dispersible in tetramethylurea (TMU) and 1,2-dichlorobenzene, forming colloidal suspensions that were stable over the course of several months. Although dispersions in toluene were not very colloidally stable, they produce visually smooth films upon drop casting that were used throughout this study unless otherwise noted. The omission of TOAB during the work-up procedure yielded

macroscopic, scroll-like pieces of WSe_2 instead of films upon deposition. The synthesis was reproducible and yielded *ca.* 150 mg WSe_2. Based on tungsten, the WSe_2 yield was ~90%, taking into account the 10% organic content observed by thermogravimetric analysis (TGA) (see Supporting Information, Figure S1). Differential scanning calorimetry (DSC) corroborated the

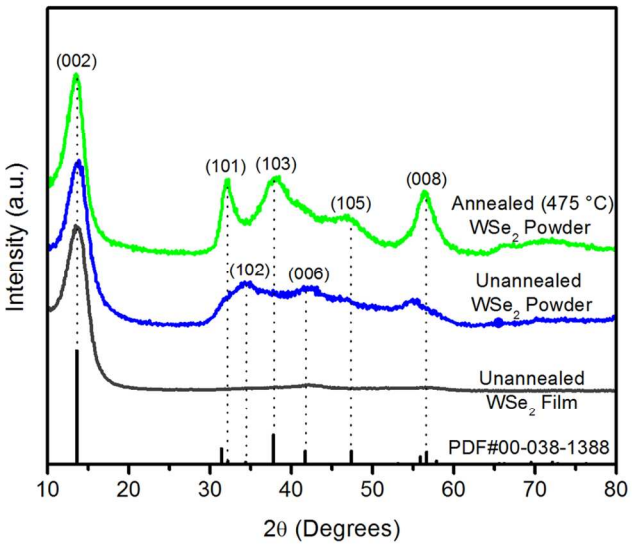

Figure 1. Film and powder XRD patterns of WSe_2 nanosheets before and after annealing at 475 °C.

endothermic loss of organic material between 250-475 °C (see Supporting Information, Figure S1).

Powder X-ray diffraction (XRD) patterns of annealed and unannealed WSe_2 nanosheets both appear to be phase pure without any crystalline tungsten oxide impurities observed in the 20-30° 2θ range (Figure 1). Despite the air stability of the product, tungsten oxide impurities were readily obtained unless strictly anaerobic conditions were employed during both the synthesis and annealing steps. The three XRD patterns in Figure 1 display a 100% intensity peak (2θ = 13.5°) indexed to the (002) reflection of the 2H-WSe_2 phase (JCPDS no. 00-038-1388).[17] Unannealed, drop-cast films displayed the (002) reflection as the prominent diffraction peak along with very small peaks at *ca.* 2θ = 42 and 57° that correspond to the (006) and (008) reflections, respectively, suggesting a strong preference for [001] orientation. Powdering the sample to reduce preferred orientation effects resulted in a diffraction pattern showing very broad diffraction peaks between 2θ = 30-60°, including the (102) reflection. Upon annealing the powdered WSe_2 nanosheets in a tube furnace for 5 min (475 °C under flowing nitrogen), additional peaks became prominent; these were indexed to (101), (103), and (105) lattice planes. To corroborate the X-ray structure data, Raman spectra of the annealed and unannealed WSe_2 films were collected. The Raman spectra of annealed and unannealed WSe_2 films both reveal a characteristic band at *ca.* 257 cm^{-1} that can be assigned to the almost degenerate E^1_{2g} and A_{1g} Raman active modes of WSe_2, while the band at *ca.* 179 cm^{-1} was assigned to the E_{1g} mode, indicative of the 2H-WSe_2 structure (see Supporting Information, Figure S2).[18] The unassigned peaks at *ca.* 127 and 319 cm^{-1} have been observed in WSe_2 single crystals[19] and are also present in the Raman spectrum of "as bought" WSe_2 powder (Alfa Aesar).

Scanning electron microscope energy-dispersive X-ray spectroscopy (SEM-EDX) and ion coupled plasma atomic emission spectrometry (ICP-AES) were used to analyze the elemental composition of the resulting WSe_2 nanosheets. Analysis of randomly selected areas gave an average W/Se composition of 1:2.0 for the unannealed material and a 1:1.8 for the annealed material (see the Supporting Information, Figure S3). ICP-AES

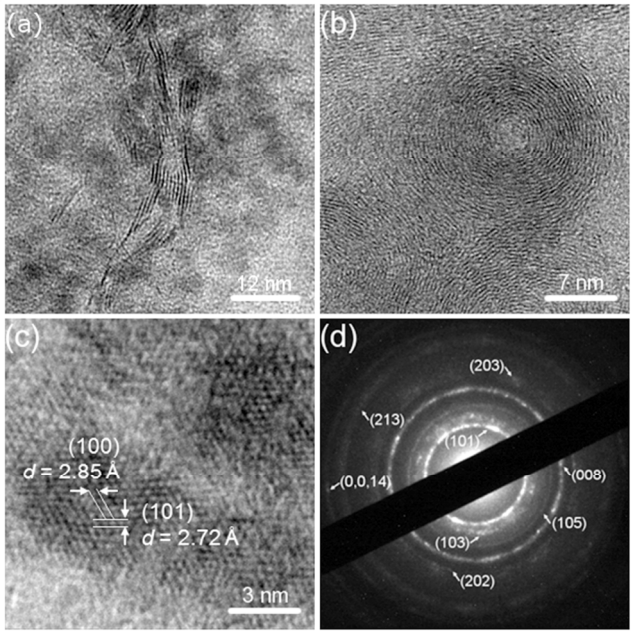

Figure 2. HR-TEM images of (a) typical WSe_2 nanosheets dried from TMU, (b) nano-onion structures of WSe_2 nanosheets dried from toluene, and (c) lattice fringes with interplanar spacings of d = 2.85 and 2.72 Å. (d) SAED pattern of annealed WSe_2 nanosheets indexed to 2H-WSe_2.

results were in close agreement, giving an average W/Se composition of 1:2.3 for the unannealed WSe_2 nanosheets.

Transmission electron microscope (TEM) analysis of the product revealed the nanosheet morphology of the WSe_2. Samples drop-cast from toluene showed some agglomerates with nano-onion structures and sheets with extended alignment (Figure 2b; Supporting Information, Figure S4), while those dried from TMU showed less extensive alignment (Figure 2a; Supporting Information, Figure S5). Individual thin sheets of various sizes were found around the agglomerates (see Supporting Information, Figure S6). A high resolution TEM (HR-TEM) image of a nanosheet displaying its (100) and (101) lattice planes (d = 2.85 and 2.72 Å, respectively) is shown in Figure 2c. Although lattice fringes were observed throughout the unannealed WSe_2 nanosheets, only a few diffuse rings were observed by selected area electron diffraction (SAED; see Supporting Information, Figure S7). This suggests that the unannealed WSe_2 nanosheets are weakly crystalline, as the powder XRD data also suggests. In contrast, more intense diffraction was observed in the SAED pattern of the annealed WSe_2 nanosheets; these were indexed in agreement with the XRD results (Figure 2d).

The electrical transport properties of the solution-processed WSe_2 nanosheets were also studied. Figure 3 shows the current-voltage (*I-V*) characteristics of an unannealed WSe_2 film that was solution deposited between two aluminum electrodes. The material was simply drop-cast from toluene and allowed to dry in air to give [001] oriented films (*vide supra*). The room temperature two-point *I-V* data of the unannealed films were collected using two types of devices with different channel dimensions to verify the measured conductivity values. Both unannealed and annealed films exhibited linear *I-V* behavior, representative of ohmic contact between the WSe_2 nanosheets and the Al electrodes. Eight devices from three different batches of WSe_2 nanosheets synthesized using identical conditions gave an

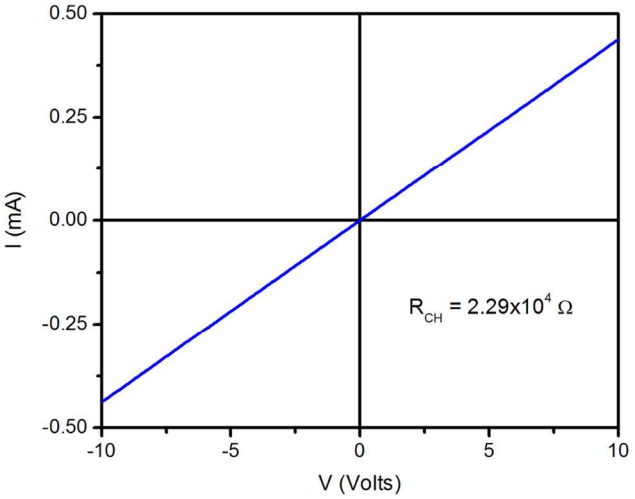

Figure 3. Room temperature two-point *I-V* measurements of an unannealed WSe_2 film using a 0.85 mm × 5.87 mm × 75 nm channel.

average conductivity of 0.6 ± 0.4 S cm^{-1}, which is in the same order of magnitude as WSe_2 single crystals (0.7 S cm^{-1})[9a] and highly conductive WSe_2 thin films (0.1 S cm^{-1}).[12a] Annealing the devices (475 °C) increased the average coductivity by two orders of magnitude to 92 ± 27 S cm^{-1}, similar to results published for highly conductive MoS_2 films (100 S cm^{-1}).[20]

In summary, a high-yielding synthesis of colloidal 2H-WSe_2 nanosheets was reported, which were shown to be phase pure by XRD. Preferential sheet alignment along the [001] direction upon solution casting was reflected in the XRD pattern and the correspondingly high conductivity values of the resulting thin films. Two-point conductivity measurements for unannealed and annealed devices gave an average value of 0.6 and 92 S cm^{-1}, respectively. Future work will focus on examining the viability of this material for use in solution-processed, nanosheet-based devices.

ASSOCIATED CONTENT

Supporting Information.
Experimental details, TGA/DSC, EDX, Raman spectra, additional TEM and SAED images of unannealed WSe_2. This material is available free of charge via the Internet at http://pubs.acs.org.

AUTHOR INFORMATION

Corresponding Author
* E-mail: brutchey@usc.edu

Notes
The authors declare no competing financial interest.

ACKNOWLEDGMENTS

This work is supported by the National Science Foundation under DMR-1205712. P.D.A. acknowledges the National Science Foundation for a Graduate Research Fellowship and R.L.B. acknowledges the Research Corporation for Science Advancement for a Cottrell Scholar Award. The authors thank P. Erwin and S. Rodney (Thompson lab), J. Liu (Zhou lab), H. Mahalingam (Steier lab), Dr. E. Couderc (Bradforth/Brutchey lab), C. Beier (Brutchey lab), and Dr. F. Rabuffetti (Brutchey lab) for both experimental assistance and helpful discussions.

REFERENCES

(1) (a) Chen, J.; Kuriyama, N.; Yuan, H.; Takeshita, H. T.; Sakai, T. *J. Am. Chem. Soc.* **2001**, *123*, 11813. (b) Zhang, Y.; Ye, J.; Matsuhashi, Y.; Iwasa, Y. *Nano Lett.* **2012**, *12*, 1136. (c) Chhowalla, M.; Amaratunga, G. A. J. *Nature* **2000**, *407*, 164. (d) Lauritsen, J. V.; Bollinger, M. V.; Laegsgaard, E.; Jacobsen, K. W.; Norskov, J. K.; Clausen, B. S.; Topsoe, H.; Besenbacher, F. *J. Catal.* **2004**, *221*, 510. (e) Justin, P.; Rao, G. R. *Int. J. Hydrogen Energ.* **2010**, *35*, 9709. (f) Dominko, R.; Arcon, D.; Mrzel, A.; Zorko, A.; Cevc, P.; Venturini, P.; Gaberscek, M.; Remskar, M.; Mihailovic, D. *Adv. Mater.* **2002**, *14*, 1531. (g) Xiao, J.; Choi, D.; Cosimbescu, L.; Koech, P.; Liu, J.; Lemmon, J. P. *Chem. Mater.* **2010**, *22*, 4522. (h) Thomalla, M.; Tributsch, H. *J. Phys. Chem. B* **2006**, *110*, 12167.
(2) (a) Morris, R. C.; Bhandari, R.; Coleman, R. V. *Phys. Rev. B* **1972**, *5*, 895. (b) Dunnill, C. W.; Edwards, H. K.; Brown, P. D.; Gregory, D. H. *Angew. Chem., Int. Ed.* **2006**, *45*, 7060.
(3) Goodson, K. E. *Science* **2007**, *315*, 342.
(4) Dominko, R.; Gaberscek, M.; Arcon, D.; Mrzel, A.; Remskar, M.; Mihailovic, D.; Pejovnik, S.; Jamnik, J. *Electrochim. Acta* **2003**, *48*, 3079.
(5) (a) Kumar, A.; Ahluwalia, P. K. *Eur. Phys. J. B* **2012**, *85*, 186. (b) Mak, K. F.; Lee, C.; Hone, J.; Shan, J.; Heinz, T. F. *Phys. Rev. Lett.* **2010**, *105*, 136805. (c) Wang, Q. H.; Kalantar-Zadeh, K.; Kis, A.; Coleman, J. N.; Strano, M. S. *Nat. Nanotechnol.* **2012**, *7*, 699.
(6) (a) Tributsch, H. *J. Electrochem. Soc.* **1978**, *125*, 1086. (b) Legma, J. B.; Vacquier, G.; Traore, H.; Casalot, A. *Mat. Sci. Eng. B-Solid* **1991**, *8*, 167.
(7) Kam, K. K.; Parkinson, B. A. *J. Phys. Chem.* **1982**, *86*, 463.
(8) Prasad, G.; Srivastava, O. N. *J. Phys. D Appl. Phys.* **1988**, *21*, 1028.
(9) (a) Agarwal, M. K.; Patel, P. D.; Vijayan, O. *Phys. Status Solidi A* **1983**, *78*, 133. (b) El-Mahalawy, S. H.; Evans, B. L. *Phys. Status Solidi B* **1977**, *79*, 713.
(10) Gamble, F. R. *J. Solid State Chem.* **1974**, *9*, 358.
(11) Bromley, R. A.; Yoffe, A. D.; Murray, R. B. *J. Phys. Part C Solid* **1972**, *5*, 759.
(12) (a) Pouzet, J.; Bernede, J. C.; Khellil, A.; Essaidi, H.; Benhida, S. *Thin Solid Films* **1992**, *208*, 252. (b) Legma, J. B.; Vacquier, G.; Casalot, A. *J. Cryst. Growth* **1993**, *130*, 253. (c) McKone, J. R.; Pieterick, A. P.; Gray, H. B.; Lewis, N. S. *J. Am. Chem. Soc.* **2013**, *135*, 223. (d) Benhida, S.; Bernede, J. C.; Delphine, S. M.; Jayachandran, M.; Sanjeeviraja, C. *Mater. Chem. Phys.* **2003**, *81*, 78. (e)

Delphine, S. M.; Jayachandran, M.; Sanjeeviraja, C. *Mater. Chem. Phys.* **2003**, *81*, 78.
(13) Huang, J. M.; Kelley, D. F. *Chem. Mater.* **2000**, *12*, 2825.
(14) Duphil, D.; Bastide, S.; Rouchaud, J. C.; Pastol, J. L.; Legendrel, B.; Levy-Clement, C. *Nanotechnology* **2004**, *15*, 828.
(15) (a) Franzman, M. A.; Perez, V.; Brutchey, R. L. *J. Phys. Chem. C* **2009**, *113*, 630. (b) Webber, D. H.; Brutchey, R. L. *Chem. Commun.* **2009**, 5701. (c) Norako, M. E.; Brutchey, R. L. *Chem. Mater.* **2010**, *22*, 1613. (d) Webber, D. H.; Brutchey, R. L. *Inorg. Chem.* **2011**, *50*, 723. (e) Norako, M. E.; Greaney, M. J.; Brutchey, R. L. *J. Am. Chem. Soc.* **2012**, *134*, 23. (f) Buckley, J. J.; Rabuffetti, F. A.; Hinton, H. L.; Brutchey, R. L. *Chem. Mater.* **2012**, *24*, 3514.
(16) Kurth, D. G.; Lehmann, P.; Lesser, C. *Chem. Commun.* **2000**, 949.
(17) Wong-Ng, W.; McMurdie, H.; Paretzkin, B.; Zhang, Y.; Davis, K.; Hubbard, C.; Alan, D.; Stewart, J. *Powder Diffr.* **1987**, *2*, 257.
(18) Mead, D. G.; Irwin, J. C. *Can. J. Phys.* **1977**, *55*, 379.
(19) Galun, E.; Cohen, H.; Margulis, L.; Vilan, A.; Tsirlina, T.; Hodes, G.; Tenne, R.; Hershfinkel, M.; Jaegermann, W.; Ellmer, K. *Appl. Phys. Lett.* **1995**, *67*, 3474.
(20) Tachibana H.; Yamanaka, Y.; Sakai, H.; Abe, M.; Matsumoto, M. *Chem. Mater.* **2000**, *12*, 854.